Impurity cations in the bulk and the {001} surface of muscovite: an atomistic simulation study

John A. Purton,[a,b] **Neil L. Allan**[a] **and Jon D. Blundy**[b]

[a]*School of Chemistry, University of Bristol, Cantock's Close, Bristol, UK BS8 1TS*
[b]*CETSEI, Department of Geology, University of Bristol, Wills Memorial Building, Bristol, UK BS8 1RJ*

Solution energies are calculated for monovalent and divalent impurities in the bulk and the {001} surface of muscovite, using atomistic simulation techniques and a consistent set of interatomic potentials. Cs^+ is the most soluble alkali metal cation. There are marked differences between the bulk and surface solution energies for the smaller univalent cations, indicating appreciable segregation to the surface. Without deprotonation of an OH group, none of the Group 1 cations are able to enter the hexagonal cavity on the mica basal plane. Small divalent cations are predicted to substitute for octahedral Al with the most favourable charge-balance mechanism involving the additional substitution of Al for Si. The solution mechanism for larger, less soluble divalent cations involves substitution for K^+, with a compensating Al/Si exchange. Where possible, results are calculated for two models, the first assuming complete ordering of Al and Si on the tetrahedral aluminosilicate sheets and the second completely random ordering. There is little difference between the values from the two models, with the exception of the {001} surface energy.

The incorporation of cation impurities in solids and at solid surfaces is crucial to many chemical and physical phenomena, ranging from high-temperature superconductivity and catalysis to trace element partitioning between co-existing phases in geochemistry. An understanding of the factors controlling this incorporation in silicate minerals has implications for processes as wide ranging as radioactive waste management and Earth differentiation. In this paper we extend our earlier work on the energetics of isovalent and heterovalent element substitution in silicates[1,2] and examine incorporation in the bulk and at the {001} surface of muscovite $KAl_{2(oct)}Al_{(tet)}Si_3O_{10}(OH)_2$, including that of cations with radioactive isotopes such as Cs^+. Muscovite is a commonly occurring mica[3] found in syenites, pegmatites and granites, in metamorphic rocks such as gneisses and schists and also in many sedimentary rocks. Weathering of aluminosilicates such as muscovite in aqueous and low-temperature hydrothermal environments leads to the formation of clays, which play an important role in defining the chemical and physical properties of sedimentary systems, and is highly relevant to our understanding of processes such as the transport of natural and contaminant species. Thus far we have not studied layered structures, which have strongly anisotropic elastic properties. Even though muscovite lacks the structural water layers important for cation absorption in clays and their plasticity when wet, we have chosen muscovite here as representative of sheet silicates with clay-related structures, as a first step towards detailed simulations of complex clays themselves.[4] Here we concentrate on the solution energies, mostly in the dilute limit, of trace element cations in the solid mineral.

Fig. 1 shows the structure of muscovite. Tetrahedral aluminosilicate sheets are formed by $(Si,Al)O_4$ tetrahedra which form a hexagonal network by sharing vertices. Sheets are arranged together in pairs such that the vertices of the tetrahedra point inwards. Al atoms cross-link these vertices, and OH groups placed inside the hexagonal rings formed by the oxygen atoms at the vertices of the tetrahedra. These Al atoms occupy octahedral sites between the two sheets in each pair. The double sheets form layers which are stacked along the *c*-axis. Layers are negatively charged and held together by charge-balancing K^+ ions in twelve-fold coordination.

In the main, the theoretical methods and computational procedures used here are identical to those employed in earlier studies of oxides and halides and have been described at length
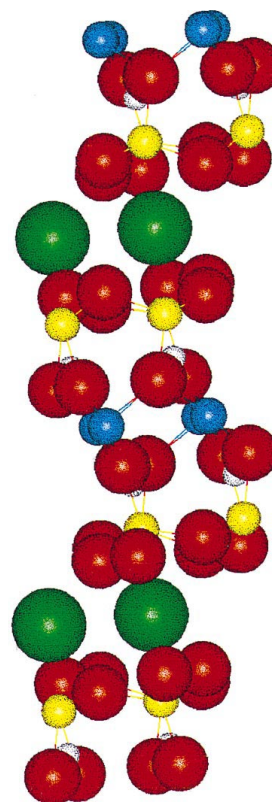

Fig. 1 Structure of muscovite. O atoms are red, the tetrahedral Si/Al atoms yellow, octahedrally coordinated Al blue, K green and H atoms grey.

elsewhere.[5–8] The application of these techniques to the simulation of trace elements in minerals such as muscovite is particularly challenging for several reasons. First, there is the problem of reliable interatomic potentials for both bulk and impurity atoms, which is particularly acute when describing the interlayer interactions. In addition there are the possible effects of Al/Si ordering. Although muscovite exhibits no long-range ordering of tetrahedral Al and Si, short-range ordering

may occur, partial evidence for which comes from NMR studies[9] indicating the absence of Al—O—Al linkages. Accordingly two sets of results are presented here, the first (the 'ordered' model) assuming a fully ordered Al/Si sublattice, and the second using a 'hybrid' model used by Pavlides and Catlow,[10] in which the same interionic potentials were used and a charge of $+3.75e$ was assigned to both tetrahedrally coordinated Al and Si. A comparison of the two sets of the results allows us to assess how sensitive the calculated energies are to the model used for the Al/Si sublattice.

We present results both for isovalent and heterovalent substitution. Compared to isovalent substitution the incorporation of ions with a charge different from that of the host cation presents several additional problems. To maintain charge neutrality, the charged defect must be accompanied by a charge-compensating defect(s). For muscovite this could be either a vacancy (e.g., one Sr^{2+} and a potassium vacancy replacing two K^+ ions) or another heterovalent cation (e.g., K^+ and Si^{4+} may be replaced together by Sr^{2+} and Al^{3+} respectively). As a result, any theoretical study must take into account both substituent and possible compensating defects, and their spatial arrangement. Since the 'ordered' model allows us to assess the energies both of vacancy compensation and coupled Al/Si substitution, our approach here and some of our conclusions differ from those of an earlier study of absorption in bulk muscovite.[10]

Muscovite is easily cleaved perpendicular to the c-direction, since the interactions between the aluminosilicate layers are much weaker than the intralayer interactions. As part of this work we consider the structure and energetics of the resulting {001} surface (Fig. 1), and relate these to the results of recent atomic force microscopy (AFM) studies. We also compare surface solution energies with those calculated for the bulk mineral.

Theoretical methods

We present only a short summary. The calculations are formulated within the framework of an ionic model; integral ionic charges are assigned based on accepted chemical valence and electron counting, i.e. $+1$ for K, $+3$ for octahedrally coordinated Al, and $2-$ for O. For the aluminosilicate layers, as already mentioned, two sets of calculations were performed, the first of which used charges of $+4$ and $+3$ for tetrahedral Si and Al, and the second an average charge of $+3.75$ for both (the 'hybrid' model). The shell model of Dick and Overhauser[11] is used to take some account of electronic polarisation.

The simulations reported in this paper are of three types: atomistic simulations of the perfect lattice, defective lattice and surface structure. Static simulations of the perfect lattice yield the crystal structure and lattice energy. In the athermal limit, the structure of the lattice is determined by the condition that it is in mechanical equilibrium, i.e.,

$$\partial E/\partial X_i = 0$$

in which E is the static contribution to the internal energy, and the $\{X_i\}$ are the variables that define the structure. Checks for dynamic stability were also carried out by confirming the absence of imaginary frequencies in the phonon spectrum. The $\{X_i\}$ consists of the three lattice vectors, the atomic positions in the unit cell, and, in the case of the shell model, the shell displacements. The last of these represents the electronic polarisation of ions which are not at a centre of inversion symmetry in the lattice and for ions such as O^{2-}, which are highly polarisable, make an appreciable contribution to the stability of the lattice, and hence to the structure and internal energy.

The most convenient approach to the treatment of defective lattices is the familiar two-region approach introduced by Lidiard and Norgett[12] (described in full by Catlow and

Mackrodt[5]), as implemented in the program CASCADE.[13] In this method the total energy of the defective system is minimized by a relaxation of the nuclear positions and shell displacements of the ions surrounding the defect. It is a reasonable assumption that this relaxation is greatest in the proximity of the defect and that the relaxations decrease fairly rapidly at distances away from the defect. The crystal is accordingly partitioned into an inner region immediately surrounding the defect, where the relaxations are assumed to be greatest, and an outer region which is only slightly perturbed. In the former the appropriate elastic equations for the force are solved explicitly, yielding the relaxed nuclear positions and shell displacements. In the outer region, however, these are estimated using a suitable approximation, in this case that suggested by Mott and Littleton.[14] Some defect energies were also evaluated using a periodic 'supercell' approach.[15] Results obtained in this way differed only slightly from those evaluated by the Mott–Littleton technique.

For atomistic simulation of surfaces the assumption is made that surfaces are planar with two-dimensional periodic boundary conditions parallel to the interface. Irregularities such as steps, kinks and ledges, which are present on real surfaces, are omitted from the present treatment. For muscovite the energy of the {001} surface was evaluated using a suitable supercell slab containing approximately 250 ions; the value thus obtained is expected to be very close to that from a two-region approach analogous to that for the defective lattice.[16] The energies of defective surfaces were also calculated by means of an appropriate supercell slab.

The success of any simulation relies on the accuracy and transferability of the short-range interatomic potentials.[17] In the main we have used a well established set of potentials and shell parameters developed by Collins and Catlow[18] and also used in ref. 10 with the additional modification to the O—H potential described in this reference. However, several new potentials were determined by empirical fitting to the lattice parameter and elastic properties of the relevant binary oxide (Table 1). This included the $K^+—O^{2-}$ potential, since we found that listed in ref. 10 gave some defect energies that were physically unrealistic.

Results

Bulk structure

Table 2 lists the calculated lattice parameters for both ordered and hybrid models. For the ordering model we have considered all possible orderings of tetrahedral Si and Al consistent with a unit cell size of 84 ions, but list results only for the lowest energy ordering shown in Fig. 2. This ordering is consistent with the observed absence of Al—O—Al links. Lattice parameters, elastic and dielectric moduli are reproduced well.

Bulk substitutions

Univalent ions. We start with univalent ion substitution and consider the reaction

$$M_2O + 2K_K \rightarrow 2M_K + K_2O \qquad (1)$$

written using Kröger–Vink notation.[19] Clearly this reaction involves not only the defect energy $E(M_K)$ but also the

Table 1 Short-range potentials used in this study that have not been previously reported. The form of the potential function is: $V = A \exp(-r/\rho) - Cr^{-6}$

interaction	A/eV	ρ/Å	C/eV Å^{-6}
$Li^+—O^{2-}$	354.01	0.3239	0.0
$K^+—O^{2-}$	680.44	0.3798	0.0
$Rb^+—O^{2-}$	919.38	0.3772	0.0

Table 2 Calculated lattice parameters and selected elastic constants for the 'hybrid' and 'ordered' models of muscovite. Only results for the lowest energy 'ordered' arrangement of tetrahedral Al and Si are given (see text). Observed structural data are from ref. 29 and elastic constants from ref. 30. For comparison a value of 5.71 has been reported[31] for the average of ε_{ii}^{0} ($i = 1, 3$) and ref. 30 gives 2.43–2.54 for the average of $\varepsilon_{ii}^{\infty}$ ($i = 1, 3$).

property	observed	hybrid model	ordered model
structure			
a	5.204	5.06	5.11
b	9.018	9.40	9.39
c	20.073	20.51	20.22
β	95.82	97.53	97.49
elastic constant			
C_{11}	18.43	16.80	17.08
C_{22}	17.84	21.72	20.32
C_{33}	5.91	4.78	4.79
C_{44}	1.60	1.02	1.10
C_{55}	1.76	1.82	1.76
C_{66}	7.24	5.69	5.49
static relative permittivity			
ε_{11}^{0}		5.71	6.19
ε_{22}^{0}		5.19	5.99
ε_{33}^{0}		4.89	5.19
high frequency relative permittivity			
$\varepsilon_{11}^{\infty}$		1.69	1.70
$\varepsilon_{22}^{\infty}$		1.74	1.75
$\varepsilon_{33}^{\infty}$		1.67	1.68

Fig. 3 Calculated solution energies (eV) vs. ionic radius[20] (Å) for substitution by +1 ions in muscovite for 'ordered' (squares) and 'hybrid' (circles) models
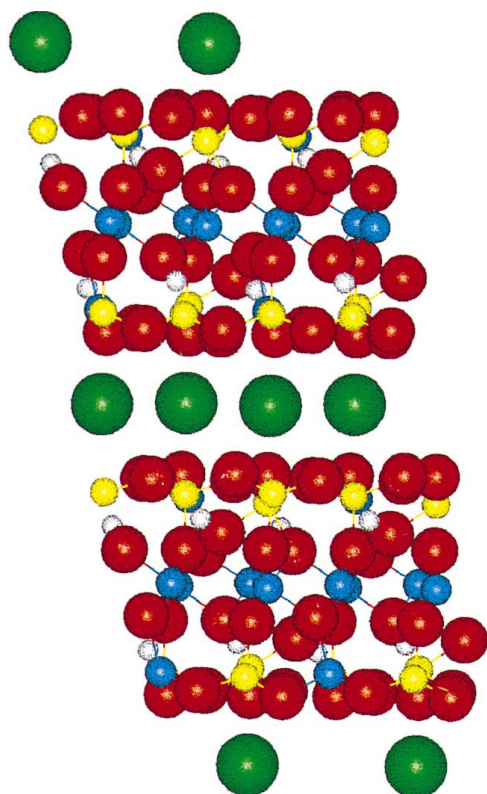

Fig. 2 Calculated lowest energy ordering of tetrahedral Al and Si. The Si atoms are yellow and the Al blue.

difference in lattice energies between K_2O and M_2O. Fig. 3 shows the variation of solution energy of M^+ as a function of ionic radius.[20] The solution energy decreases from Li^+ to Cs^+ with negative solution energies for the two largest alkali metal cations, Rb^+ and Cs^+. There is little difference between the values for the ordered and hybrid models. The results for Cs^+ compare with the value of $+0.69$ eV calculated in ref. 10,
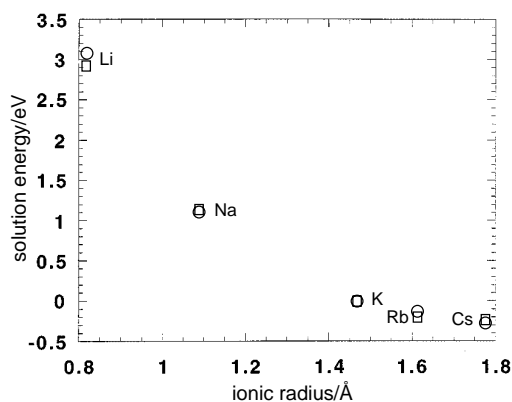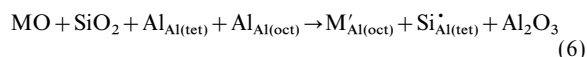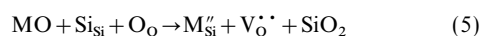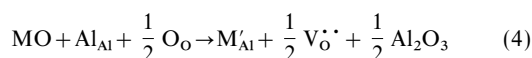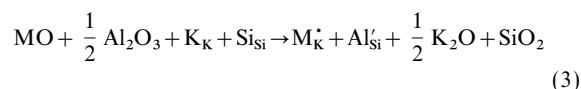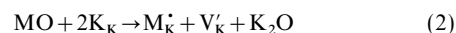
illustrating the sensitivity of the results to the potentials employed. It is interesting that our calculated solution energies do not agree with the general rule of thumb that the most soluble dopants are those closest in size to the host cation (K^+). This contrasts with those calculated in our earlier work on non-layered silicate minerals[1,2] and presumably reflects the weak interlayer interactions in muscovite, which do not inhibit an increase in the interlayer separation. Of course, we have not considered hydration in our model, but nevertheless it is worth noting that exchange of monovalent ions in hydrated clays often follows the selectivity sequence:[21] $Cs^+ > Rb^+ > K^+ > Na^+ > Li^+$.

In principle other modes of solution are possible for univalent cations, involving substitution of potassium for aluminium and silicon with oxygen vacancies as the compensating defect that preserves electrical neutrality. The resulting calculated solution energies all lie much higher in energy than those of the isovalent replacement of K^+ and so are not considered further.

Divalent ions. There are several possible sites for divalent ion substitution: potassium, aluminium or silicon. In addition, as we have already stressed, electroneutrality requires that incorporation of charged defects must be accompanied by charge-compensating defect(s). For M^{2+} impurities, likely possibilities include: (i) cation vacancies or coupled Al/Si substitution when the M^{2+} ion occupies the K^+ site [reactions (2) and (3)]; (ii) anion vacancies accompanying substitution of M^{2+} for Al^{3+} or Si [reactions (4) and (5)]; (iii) substitution for the octahedrally coordinated Al^{3+} accompanied by replacement of a tetrahedrally coordinated Al^{3+} by Si^{4+} [reaction (6)]:

$$MO + 2K_K \rightarrow M_K^{\bullet} + V_K' + K_2O \qquad (2)$$

$$MO + \frac{1}{2}Al_2O_3 + K_K + Si_{Si} \rightarrow M_K^{\bullet} + Al_{Si}' + \frac{1}{2}K_2O + SiO_2 \qquad (3)$$

$$MO + Al_{Al} + \frac{1}{2}O_O \rightarrow M_{Al}' + \frac{1}{2}V_O^{\bullet\bullet} + \frac{1}{2}Al_2O_3 \qquad (4)$$

$$MO + Si_{Si} + O_O \rightarrow M_{Si}'' + V_O^{\bullet\bullet} + SiO_2 \qquad (5)$$

$$MO + SiO_2 + Al_{Al(tet)} + Al_{Al(oct)} \rightarrow M_{Al(oct)}' + Si_{Al(tet)}^{\bullet} + Al_2O_3 \qquad (6)$$

Note that the hybrid model which uses an average charge for tetrahedral Si and Al cannot be used to calculate solution

energies for reactions (3)–(6), and so with this model we are restricted to consideration of only reaction (2).

The lowest solution energies by far were obtained for reactions (3) and (6) since cation and anion vacancy creation are both very expensive. The solution energies for both reactions are plotted for a wide range of divalent cations in Fig. 4. The solution energies for reaction (3) show a steady decrease with increasing ionic radius, with the lowest value for the largest divalent cation studied, Ba^{2+}. For reaction (6) the solution energies increase with the size of the cation and this is the favoured solution mechanism for ions smaller than Sr^{2+}. The calculated solution energies for Mg^{2+}, Co^{2+} and Fe^{2+} are negative. Thus the mode of solution is predicted to switch from reaction (6) to (3) as the ionic radius increases, which is consistent with experimental data on the partitioning of trace-element cations between muscovite and hydrous silicate melts[22] which show that Ca^{2+} and Sr^{2+} are considerably less soluble in muscovite than either Mg^{2+} or Ba^{2+}.

For reaction (2), for which solution energies can be calculated using either the ordered or hybrid models, there are only small differences between the resulting values and the same qualitative trends are reproduced in both sets of results. We must emphasise, though, that reaction (6) or reaction (3), not reaction (2), is the calculated lowest energy solution mechanism of those considered.

Surface structure and surface substitution

No simple cut parallel to the *ab*-plane produces a non-dipolar surface, and therefore a non-infinite surface energy.[23] Accordingly we have constructed a non-dipolar {001} surface by moving half of the K^+ ions. The resulting stacking sequence and the surface termination is shown in Fig. 5. The outermost layers of the supercell slab are thus comprised of K^+ ions. The resulting surface energies using the ordered and hybrid models are 1.09 J m^{-2} and 0.55 J m^{-2} respectively. For the first time we see a relatively large difference between the results from ordered and hybrid models. The relaxation of the oxygen ions is small, consistent with the conclusions from AFM.[24] The AFM images do not show any spots corresponding to the K^+ ions;[24] we find the activation energy for K^+ diffusion to be less than 0.5 eV and so a possible explanation for the AFM results is that the scanning tip displaces the K^+ ions.

For the calculations of solution energies at the surfaces, care was taken to ensure that substitutions were carried out both at the top and the bottom of the slab so that the zero dipole moment perpendicular to the surface was preserved. The resulting solution energies for the substitution of K^+ by other univalent ions at the {001} surface are shown in Fig. 6 and it is clear that there are significant differences between the surface

Fig. 5 Reconstructed {001} surface of muscovite. O atoms are red, the tetrahedral Si/Al atoms yellow, octahedrally coordinated Al blue, K green and H atoms grey. The surface is at the top of the figure.

Fig. 6 Calculated solution energies (eV) *vs.* ionic radius (Å) for substitution by +1 ions at the reconstructed {001} surface of muscovite for (*a*) 'hybrid' and (*b*) 'ordered' models. Open circles denote surface solution energies and squares the corresponding bulk values.
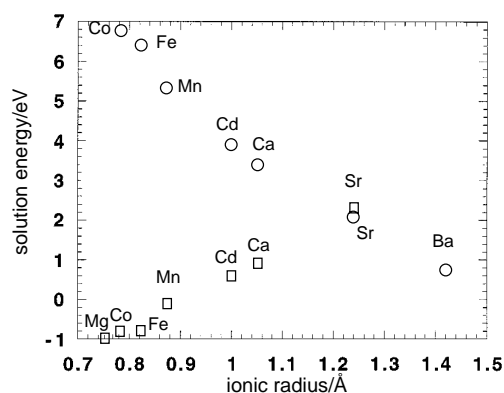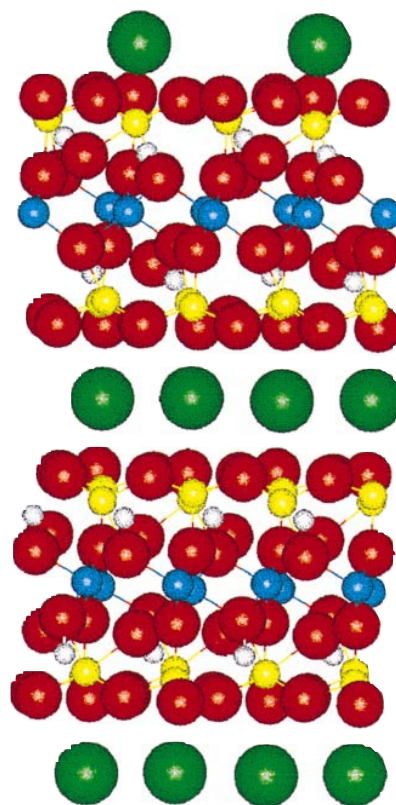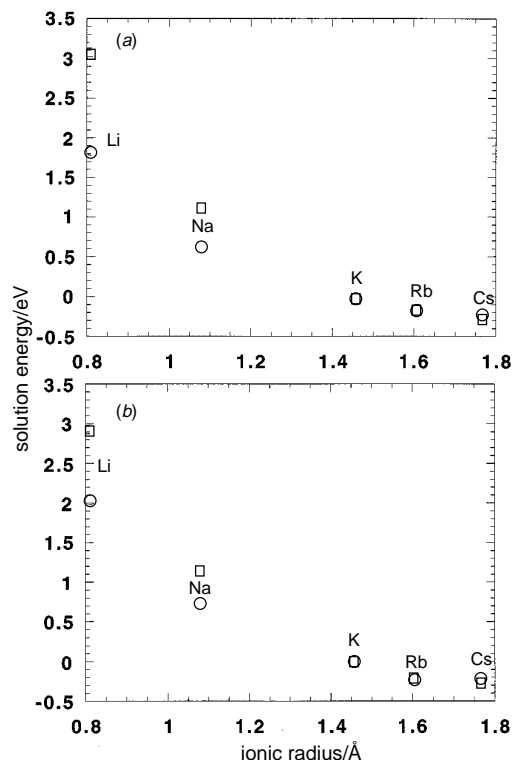

Fig. 4 Calculated solution energies (eV) *vs.* ionic radius (Å) for substitution by +2 ions in muscovite ('ordered' model only) according to reactions (3) (circles) and (6) (squares)

and the bulk values. Cations smaller than K^+ are more soluble at the surface and larger ones slightly less soluble. The same trends are observed in both ordered and hybrid models (see Fig. 6).

There has been considerable controversy regarding the position of Li^+ ions in 2:1 type sheet silicates.[25] Our calculated lowest energy minimum position for the Li^+ shows that, in the absence of hydration effects (proton release), it does not sit in the hexagonal cavity on the mica basal plane. Li^+ occupies an analogous position to K^+, but lies closer to the nearest oxygen.

Conclusions

We have shown that atomistic simulation techniques with a consistent set of interatomic potentials can be applied to complex minerals such as muscovite. These calculations are relatively cheap and the approach highly specific. We have calculated solution energies for monovalent and divalent impurities in the bulk and at the {001} surface of muscovite. Of the Group 1 cations Cs^+ is the most soluble. For the smaller univalent cations, there are marked differences between the bulk and surface solution energies, indicating appreciable segregation to the surface. Without deprotonation of an appropriate hydroxy group none of the Group 1 cations are able to enter the hexagonal cavity on the mica basal plane. Small divalent cations are predicted to be soluble, by means of a coupled substitution of the divalent ion for Al and Si for Al. The ease of incorporation of Mg^{2+} is consistent with the trace-element partitioning data[26] and the occurrence of an extensive solid solution between muscovite and phengite $K(Mg_{0.5}Al_{1.5})(Al_{0.5}Si_{3.5}O_{10})(OH)_2$ in metamorphic rocks at high pressure.[27] The mechanism for larger divalent cations is different, involving substitution for K coupled with Al substitution for Si.

For the properties considered here, with the exception of the {001} surface energy, there is little difference between the results obtained using the ordered and the hybrid models. The individual energies that contribute to the solution energies (*e.g.*, the relaxation energy surrounding the defects) differ much more from the one model to the other, and so the apparent good agreement between the two appears to rely on the cancellation of different energy contributions. The hybrid model cannot be used for modes of solution involving Al replacing Si, or *vice versa*, which we have seen is the lowest energy mode for the incorporation of divalent ions in muscovite.

The available trace-partitioning data for muscovite[22] indicates that of the alkali metal cations, the partition coefficient for Rb^+ ($[Rb^+]_{mineral}/[Rb^+]_{melt}$) is the largest, whereas the lowest calculated solution energy is for Cs^+. This suggests a need to account explicitly for the melt when rationalising trace-partitioning data. We must caution also that we have considered only thermodynamic aspects of impurity incorporation, ignoring possible hydration effects. In applications kinetic factors may also be important, and consideration of all of these will form part of our future work.

References

1 J. A. Purton, N. L. Allan, J. D. Blundy and E. A. Wasserman, *Geochim. Cosmochim. Acta*, 1996, **60**, 4977.
2 J. A. Purton, N. L. Allan and J. D. Blundy, *Geochim. Cosmochim. Acta*, in press.
3 See, for example, *Rev. Mineral.*, ed. S. W. Bailey, 1984, **13**.
4 For an overview of theoretical approaches to the modelling of phyllosilicates, see W. F. Bleam, *Rev. Geophys.*, 1993, **31**, 1.
5 C. R. A. Catlow and W. C. Mackrodt, in *Computer Simulation of Solids*, ed. C. R. A. Catlow and W. C. Mackrodt, Springer-Verlag, Berlin–Heidelberg–New York, 1982, ch. 1.
6 C. R. A. Catlow, in *Solid State Chemistry: Techniques*, ed. A. K. Cheetham and P. Day, Clarendon Press, Oxford, 1987, ch. 7.
7 For example, *Computer Modelling in Inorganic Crystallography*, ed. C. R. A. Catlow, Academic Press, San Diego–London, 1996.
8 For previous mineral simulations see, for example, M. J. Sanders, M. Leslie and C. R. A. Catlow, *J. Chem. Soc., Chem. Commun.*, 1984, 1273; C. R. A. Catlow and G. D. Price, *Nature* (*London*), 1990, **347**, 243; A. Patel, G. D. Price and M. Mendelssohn, *Phys. Chem. Mineral.*, 1991, **17**, 690; B. Winkler, M. T. Dove and M. Leslie, *Am. Mineral.*, 1991, **76**, 313; S. C. Parker and G. D. Price, *Adv. Solid State Chem.*, 1989, **1**, 295.
9 J. Sanz and J. M. Serratosa, *J. Am. Chem. Soc.*, 1984, **106**, 4790; C. P. Herrero, J. Sanz and J. M. Serratosa, *Solid State Commun.*, 1985, **53**, 151.
10 P. Pavlides and C. R. A. Catlow, *Mol. Phys.*, 1994, **81**, 1269.
11 B. G. Dick and A. W. Overhauser, *Phys. Rev.*, 1958, **112**, 90.
12 A. B. Lidiard and M. J. Norgett, in *Computational Solid State Physics*, ed. F. Herman, W. W. Dalton and T. R. Koeler, Plenum, New York, 1972, p. 385.
13 M. Leslie, SERC Daresbury Laboratory Technical Memorandum DL/SCI/TM31T, 1982. A region *I* size of 8 Å was used throughout.
14 N. F. Mott and M. T. Littleton, *Trans. Faraday Soc.*, 1938, **34**, 485.
15 M. Leslie and M. J. Gillan, *J. Phys. C*, 1985, **18**, 973.
16 For example, D. H. Gay and A. L. Rohl, *J. Chem. Soc., Faraday Trans.*, 1995, **91**, 925.
17 For earlier work considering largely only the electrostatic contribution to the total energy, see, *e.g.*, H. D. B. Jenkins, in *Computer Simulation of Solids*, ed. C. R. A. Catlow and W. C. Mackrodt, Springer-Verlag, Berlin–Heidelberg–New York, 1982, ch. 16; R. F. Giese Jr., *Rev. Mineral.*, 1984, **13**, 105.
18 D. R. Collins and C. R. A. Catlow, *Am. Mineral.*, 1992, **77**, 1172. The potential cutoff used is 12 Å.
19 F. A. Kroger and H. J. Vink, *Solid State Phys.*, 1956, **3**, 307.
20 For the ionic radii we have taken the values for six-fold coordination from R.D. Shannon, *Acta Crystallogr., Sect. A*, 1976, **32**, 751. As suggested by Babel (D. Babel, *Z. Anorg. Allg. Chem.*, 1969, **369**, 117) ionic radii for the twelve-coordinate M^+ and M^{2+} ions have been assumed to be 6% greater than the radii for the same ions when octahedrally coordinated.
21 For example, M. M. Morel and J. G. Hering, *Principles and Applications of Aquatic Chemistry*, Wiley, New York, 1993, p. 557.
22 J. Icenhower and D. London, *Am. Mineral.*, 1995, **80**, 1229.
23 F. Bertaut, *Compt. Rend.*, 1958, **246**, 3447.
24 S. Nishimura, S. Biggs, P. J. Scales, T. W. Healey, K. Tsunematsu and T. Tateyama, *Langmuir*, 1994, **10**, 4554.
25 U. Hofmann and R. Z. Klemen, *Z. Anorg. Allg. Chem.*, 1950, **262**, 95; R. Green-Kelly, *Mineral. Mag.*, 1955, **30**, 604; R. Tettenhorst, *Am. Mineral.*, 1962, **47**, 769; W. F. Jaynes and J. M. Bigham, *Clays Clay Miner.*, 1987, **35**, 440.
26 M. Volfinger, *Bull. Soc. Fr. Minéral Cristallogr.*, 1975, **98**, 49.
27 C. V. Guidotti, *Rev. Mineral.*, 1984, **13**, 357.
28 R. D. Shannon, *Acta Crystallogr., Sect. A*, 1976, **32**, 751.
29 R. A. Knurr and S. W. Bailey, *Clays Clay Miner.*, 1986, **34**, 7.
30 M. T. Vaughan and S. Guggenheim, *J. Geophys. Res.*, 1986, **92**, 4657.
31 M. F. Golop, A. B. Nalivken and A. Vokemenstev, *SER Shrencat Natures*, 1968, **22**, 3.